Contribution to Accurate Spherical Gold Nanoparticles Size Determination by Single Particle Inductively Coupled Mass Spectrometry: a Comparison with Small Angle X-ray Scattering

Valérie Geertsen, Elodie Barruet, Frédéric Gobeaux, Jean-Luc Lacour, Olivier Tache

Contribution to Accurate Spherical Gold Nanoparticles Size Determination by Single Particle Inductively Coupled Mass Spectrometry: a Comparison with Small Angle X-ray Scattering

Valerie Geertsen[a], Elodie Barruet[a], Frédéric Gobeaux[a], Jean-Luc Lacour[b] and Olivier Taché[a]

a : Nimbe, CEA, CNRS, Université Paris Saclay, 91191 Gif Sur Yvette, France

b : Den - Service d'Etudes Analytiques et de Réactivité des Surfaces (SEARS), CEA, Université Paris-Saclay, F-91191, Gif-sur-Yvette, France

Corresponding author : Valérie Geertsen

Abstract

Small Angle X-rays Scattering Spectroscopy (SAXS) is the method of choice for nanoparticle diameter and concentration determination. It is metrologically traceable for spherical nanoparticle mean diameter determination and does not require any sample preparation or calibration. On the other hand, Single Particle ICPMS (SPICPMS) is still under developments and requires involved process clarification and accuracy improvement. The strategy of this study is the comparison of the two techniques to study comprehensively SPICPMS performance and observe phenomena otherwise hidden.

6 spherical gold nanoparticle suspensions distributed over a large size range (30, 50, 60, 80,100 and150 nm) are studied as standards. Potential matrix effect are eliminated by stabilizing nanoparticles with chitosan in HCL. Chitiosan encapsulates nanoparticles, stabilizes their dispersion and protects them from dissolution.

Detection counting/analog threshold and timeout appear as the relevant parameters for transient signals. They show an influence not only on mean signal but also on signal distribution. The detection tuning proposed allow to linearly calibrate the nanoparticle distribution signal to cubed diameter over the entire range studied with no sensitivity diminution.

Comparing the 3 classical transport efficiency methods, size transport efficiency is shown as the most accurate. The new procedure is validated analyzing three gold nanoparticles suspensions (135, 40 and 50nm). The results are consistent with SAXS measurements.

Introduction

Nanometrology is an essential catalyst to nanotechnology development. Depending on requirements, nanometrology refers to measurements of size, surface, chemical and isotope compositions, electrical, mechanical, magnetic properties, *etc*... which must be provided with estimates of accuracy and repeatability. Nanometrology includes therefore a large variety of characterization techniques such as those listed by the Nanodefine European Project consortium[1] or the OECD Testing Program[2]. Among these measurements, nanoparticle size and nanoparticle size distribution are of the utmost importance as nanomaterial definitions are mostly based on size.

There are multiple ways to categorize nanoparticle size determination techniques. For instance, nanoparticle sizing principles can be distinguished according to their sampling methods (counting, ensemble)[2]. Counting methods, such as Single Particle Inductively Coupled Mass Spectrometry (SPICPMS) or imaging techniques, measure individual nanoparticles to build size distribution diagrams. Ensemble methods measure all nanoparticles simultaneously. Size distribution is then extracted from features of the entire sample signals, assuming that each size distribution fraction contributes independently and linearly[1].

Among the ensemble methods, small angle X-ray scattering (SAXS) provides total surface and gyration radius of primary particles as well as radius of gyration and inner fractal structure of aggregates[3]. It can also evaluate nanoparticles concentration in a liquid suspension[4]. SAXS is a metrologically traceable technique for mean diameter determination of spherical nanoparticles that is traceable to realizations of the SI unit “metre”[5]. It requires therefore no calibration by reference particle sample.

Although SPICPMs is not a metrologically traceable technique, it has many strengths to become a useful complement of more established nanoparticle characterization methods such as SAXS and microscopy. It is in particular the only technique that can characterize single nanoparticle chemical and isotope composition. The latter is rarely mentioned but nanoparticle isotope measurement is a subject of great importance as isotope nanotoxicology is the most reliable way to study nanoparticle environmental impact[6]. It can also measure highly dilute nanoparticles suspensions which is not the case for Dynamic Light scattering (DLS) or SAXS. Finally, ICPMS analyzes inorganic ions in liquid solution over a very large range of concentration which should allow SPICPMS to provide linear diameter measurement range over at least 3 orders of magnitude. This last point should be underlined as nanoparticles are often aggregated. Depending on sample preparation, SPICPMS could thus measure both primary particles and aggregate sizes.

Despites its strengths and the fact that its feasibility has already been demonstrated a decade ago[7], SPICPMS is still under development. Its ability to measure quantitatively and accurately nanoparticle suspensions has never been to our knowledge really demonstrated, even if it is applied to numerous toxicological and environmental studies[8]. D. Montaño and co-authors have listed in a very exhaustive review the pressing issues facing the technique if it is to be used for routine analysis[9]: lack of sensitivity (especially for light element such as silicon), lack of suspension reference materials, a need

of validated sample preparations and matrix effect evaluations for minimal sample perturbation and better accuracy, a better knowledge and accuracy of transport efficiency, and finally a better control of transport, ionization and sampling processes along the droplet trajectory from the nebulizer and into ionic cloud inside the plasma ...

This work proposes a comprehensive confrontation of quadrupole SPICPMS with SAXS in order to, investigate the method, better understand involved mechanisms and solve some of the aforementioned difficulties. SPICPMS has already been compared to other techniques[10] but to our knowledge never comprehensively to SAXS even if it is the method of choice for nanoparticle characterization. This study is realized through the analysis of 6 gold nanoparticle suspensions distributed over a large range of size (30-150nm). This point is essential and has to be highlighted as most studies are realized on smaller size ranges and with fewer suspensions. Spherical gold nanoparticles are chosen here being the most studied suspensions and the most commercially popular. Each suspension is fully characterized in terms of size and concentration by SAXS and DLS before being considered as standard for SPICPMS. SPICPMS potential matrix effects are for the first time eliminated through a nanoparticle stabilization in HCl. Nanoparticle transport efficiency is studied under these optimized operating conditions and the different calculations methods proposed in the literature are evaluated in terms of reproducibility. The nanoparticle suspension calibration curve being linear to the square of the particle diameter and not to the cube, this demonstrates that only a portion of the nanoparticle ionic cloud is detected. Quadrupole ICPMS detection issues have already been questioned especially for large signals but to our knowledge the problem has not been solved. A detection tuning methodology is proposed resulting over the entire nanoparticle diameter range in a linear calibration curve as well as a symmetrization of nanoparticle signal distribution. As a validation, the new procedure arising from this SAXS and SPICPMS comparison is applied to by the analysis of three additional commercial suspensions of gold nanoparticles (135nm, 40nm and ultra uniform 50nm).

Experimental Section

Chemicals

High-viscosity chitosan and 30, 50, 60, 80, 100, and 150 nm citrate-stabilized gold nanoparticles suspensions in H_2O are purchased from Sigma Aldrich. Water suspensions of 120 and 135 nm citrate stabilized gold nanoparticles are from Nanopartz Inc. Water suspensions of 40nm and ultra uniform 50nm citrate and PEG stabilized gold nanoparticles are from NanoComposix. HCl, supplied from Sigma Aldrich, is distilled prior to use. Nanoparticles stock suspensions are shaken vigorously for several minutes before dilution. Dilutions are performed in PFA vials by weight dilution in HCl 2%, Chitosan 1/1000 w/w. Standard gold solutions are prepared by weight dilution in HCl 2%, chitosan 1/1000 w/w of standard 10 000 mg/L Au (Spex-CertiPrep, Metuchen, USA).

Instrumentation

Transmission electron microscopy (TEM) is performed on a Philips CM12 electron microscope operated at 80 kV. A nanoparticle suspension drop is deposited on a copper grid covered with a carbon film (Agar Scientific). The excess liquid is blotted off with paper filter after about 30 seconds.

DLS measurements are performed with a Nanosizer (Malvern) in H2O or HCl 2%, chitosan 1/1000 w/w.

SAXS measurements are performed with a Xeuss 2.0 (Xenocs) equipped with a Cu microfocus X-Ray source with an incident beam size of 0.6 mm x 0.6 mm providing 6.10^6 ph/s. Absolute intensities (allowing nanoparticles concentration determination) are obtained by classical normalization[11]. By measuring transmitted beam ϕ_0 and scattered x-rays Cij with the same detector, and assuming the source stability (around ±1% during acquisition dt), intensities[4] can be simplified and calculated as :

$$\mathrm{I(q)} = \frac{\mathrm{Cij}}{\phi_0} \cdot \frac{1}{\mathrm{dt}} \cdot \frac{\mathrm{D}^2}{\mathrm{p}^2} \cdot \frac{1}{\mathrm{thickness}} \qquad (1)$$

Where D is the detector to sample distance, p is the detector pixel size and *thickness* is the sample thickness.

Nanoparticles suspensions are placed in Kapton sealed tubes (560, Microlumen) of known internal thickness (1.42mm +/- 0.01mm). The tubes fabrication extrusion process enables a very good thickness repeatability. Thickness can also be evaluated with a good accuracy measuring water transmission. Samples are placed at the atmospheric pressure. To reduce the small additional angle scattering signal by air, sample zone width is reduced to only 2 cm with a home-made instrument modification. The instrument windows are replaced by non-scattering foils (Nalophan). Every SAXS size determination are repeated keeping sample holder, acquisition time and kapton tube batch unchanged for both nanoparticle suspension and solvent (water or chitosan in HCl). The sample to detector distanced *D* is 249 cm in high resolution mode. Q axis is calibrated by observing the same

sample at different distances. Distance being the only varying parameter, it can be precisely measured in meter. Images are acquired with a Pilatus (Dectris) 1M detector with a pixel size of 172µm. Data are processed, except for the 50nm standard, with the freely available laboratory-made python PySaxs[11] software, that provides data corrections and operations from image averaging to absolute scaling. Mean diameter determination is obtained fitting data with a polydisperse sphere size and Gaussian distribution SAXS model. This model takes into account mean diameter, polydispersity, nanoparticle number concentration, beam convolution, scattering length density of the spheres (1.31×10^{12} cm^{-2}) and medium (water : 9.42×10^{10} cm^{-2}). The 50nm standard is processed with MC SAXS, a Monte Carlo algorithm, its size distribution being significantly different from Gaussian[12].

The quadrupole ICPMS is an iCAPQ (ThermoElectron) classically equipped with a glass nebulization chamber using a Peltier cooler. It is tuned in high matrix mode, with a dwell time set to 7ms unless other value specified. The sample is nebulized via a PFA-ST nebulizer in the range of 100 to 250µL/min (Elemental Scientific) or a conical 1mL/min glass nebulizer (Glass Expansion). Sampling depth is set at 5, the optimal position for gold on the instrument[13]. Data are acquired via the ThermoElectron software plugin NPQuant and treated by a custom-made Python software because of the large quantity of data generated by this method. Nanoparticle events are distinguished from the background by comparison with the blank intensity mean value plus 5 σ except for unknown sample determinations of where it is set to 4700cps. If two consecutive data are considered as nanoparticle events, the values are summed[14]. The whole procedure has been validated by comparison with the calculation spreadsheet proposed by Peters *et al*[15].

Results and discussion

Sample characterization

The development of SPICPMS for metrological purposes requires comparison with other analytical techniques. Indeed, the method is based on external calibration and there is, to our knowledge, no commercial suspension certified in concentration and diameter. To evaluate SPICPMS performance, it is then mandatory to access a large variety of, if not certified then well-characterized monodisperse suspensions. The strategy of this study is therefore to collect accurate characterization measurements to studying comprehensively SPICPMS performances and observe phenomena otherwise hidden if working only with supplier data.

The important parameters, assuming that nanoparticles are spherical, are size distribution (i.e. average value and standard deviation) and concentration. The definition of size is technique dependent. SPICPMS measures for each nanoparticle a number of atoms that is transformed into an equivalent diameter assuming the density. TEM gives access to the direct measurement of the diameter of a gold sphere projection on a plane surface. (Figure 1). DLS measures the suspension average hydrodynamic diameter which is larger than the average diameter of the gold atom spheres.

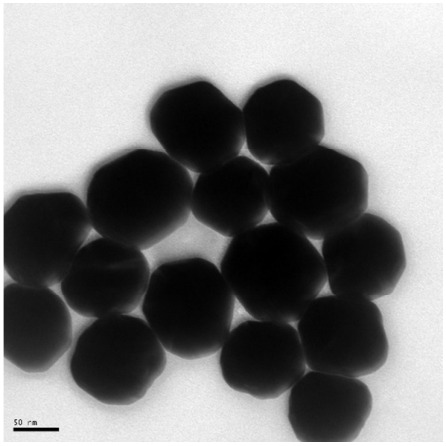

Figure 1. 100nm gold nanoparticle suspension by TEM

SAXS measures the interaction between X-rays and matter to investigate incompletely homogenous materials structures by recording scattering intensity[16]. (Figure 2). Photons interact with electrons and provide information about the fluctuations of electronic densities in the matter. The intensity pattern of the scattered radiation is treated to extract information on particle size, size distribution, shape and nanostructure. There is no sample preparation, hence no sample disturbance. It requires no calibration.

SAXS is the method of choice for nanoparticle diameter determination. Experimental uncertainties depend on few parameters (x-ray wavelength, sample to detector distance, beam divergence,…) as well described by Brian Pauw[17]. By using a well-known calibrant[18], mean diameter uncertainty is

estimated below 0.5%. Size distribution depends on model fitting method. The accuracy of the distribution itself reaches about 10%.

SAXS number concentration uncertainty is generally estimated at 10%.

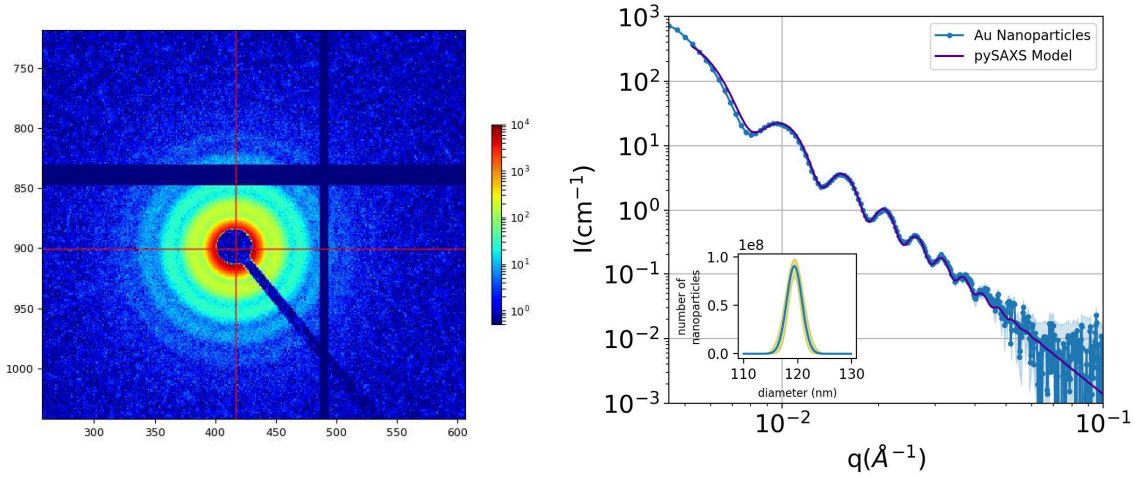

Figure 2. Typical 2D SAXS pattern of a 120nm spherical gold nanoparticles detector image. Right: Corresponding radial averaging in absolute intensity (blue line), continuous purple line: sphere Gaussian distribution fitting. Inset: diameter distribution derived from the model.

Table 1. Nanoparticle stock suspensions characterizations. SAXS: number-weighted mean diameters, Gaussian distribution standard deviations, concentrations. DLS: intensity mean diameter and polydispersity index. a: calculated from SAXS volume-weighted nanoparticle mean diameter and ICPMS gold ions concentration measured after aqua regia nanoparticle dissolution.

	Provided by Supplier	Measured by SAXS			Measured by SAXS+ICPMS	Measured by DLS	
Nanoparticles	[AuNPS] p/mL	d (nm)	σ (nm)	[AuNPS] p/mL	[AuNPS][a] p/mL	d (nm)	σ (nm)
30nm	1.8E+11	28.3	4	1.6E+11	1.7E+11	50.7	21
50nm	3.5E+10	53.3	6.5	2.8E+10	3.1E+10	64.4	24
60nm	1.9E+10	57.1	7.7	1.5E+10	1.8E+10	81.5	30
80nm	7.8E+09	78.2	9.4	5.9E+09	7.3E+09	102.6	33
100nm	3.8E+09	96.6	10.6	4.0E+09	4.4E+09	121	35
150nm	3.6E+09	142.5	13	2.4E+09	3.1E+09	178	48

Table 1 sums up nanoparticle suspension characterization in diameter by SAXS and DLS as well as concentration by SAXS and SAXS+ICPMS and compares them to supplier specifications. It shows that deviations from supplier measurements can be sizable, both for diameter and concentration. DLS diameter values are logically much larger than SAXS measurements. Comparing concentration

determinations, meaningful deviations are also observed. Looking in more details, the discrepancy between SAXS concentration measurements and SAXS+ICPMS measurements could even appear as incoherent assuming classical measurement uncertainties for both SAXS and ICPMS. The reason for this could be that gold concentration determination by ICPMS after dissolution measures gold ions resulting from both nanoparticles and dispersed gold mini clusters resulting from synthesis that are too small to be detected, but inducing probable concentration overestimates.

From these results, it can be concluded that diameter and concentration determinations by SAXS of commercial suspensions are mandatory if these suspensions are to be used as size or transport standards. Concentration values impact indeed number transport efficiency directly and hereafter the entire analytical process. In the rest of this work, SAXS determinations are preferred for both diameters and concentrations.

Stabilization

SPICPMS requires a drastic dilution of sample suspensions to analyze one nanoparticle at a time. Because solid particle dispersions in liquid is not a stable state of matter, highly diluting suspensions generally leads to destabilization and even to dissolution. A balance has to be struck, diluting suspensions (typically 25000 p/mL) just enough to minimize the probability of presence of several nanoparticles in the plasma and not too much to reduce destabilization. The literature reports that SPICPMS analysis is classically performed in water[9]. Unfortunately diluting in water avoids dissolution but not aggregation or sedimentation. Considering gold nanoparticles, these are always coated by organic molecules to eliminate aggregation. Those organic molecules exist in equilibrium between nanoparticle surfaces and liquid bulk and this equilibrium is destabilized when diluting heavily in pure water. This disequilibrium can also, in our experience, lead to long-term instrument contamination. In commonly used SPICPMS protocols, samples are analyzed in pure water but standard solutions calibrations are performed as usual in acidic media. This can induce matrix effects suspicions as already pointed out by Montaño[9] *et al*. Diluting sample as little as possible also has instrumental consequences. Analyses need to be performed at high detection speed (short dwell time) to minimize, amongst others, the probability of aggregating two close nanoparticle signal spikes as one. For most instruments like ours, short dwell times have a detrimental effect on signal stability and accuracy and lead to a loss of information due to mass spectrometer settling times and data processing. It can be concluded from all these considerations, that a procedure improvement would consist here in stabilizing gold nanoparticles down to very low concentrations to enable acquisition with long dwell times and analyze both standard solutions and nanoparticle suspensions in the same hydrochloric media. A stabilizer is then required.

Chitosan is a naturally occurring polymer that is soluble and stable in hydrochloric acid[19]. Its affinity for gold[20] has often been reported, making it a good candidate for gold nanoparticle stabilization. To validate its performances, nanoparticle suspensions are first diluted by a factor 10 in HCl 2%v/v in the presence of chitosan and analyzed by DLS and SAXS. It appears that suspensions are stable for a least 1 week whereas dilution in HCl alone produces fast sedimentation and probable dissolution. Measuring hydrodynamic diameters that include both gold nanosphere and chitosan coating, DLS

shows as expected a very large size increase compared to stock water suspensions. The average diameter increases from about 120nm to above 330nm. Chitosan being invisible to SAXS, no diameter modification is found demonstrating the absence of aggregation or dissolution. The combination of all these observations indicates that chitosan encapsulates nanoparticles, stabilizes their dispersion in the liquid and protects them from dissolution.

The influence of chitosan is also studied by ICPMS. Chitosan addition to hydrochloric acid shows no influence on standard solution calibration. Blank signal average and standard deviation are comparable to hydrochloric acid alone. Nanoparticle average signal intensity remains stable when H_2O is replaced by chitosan in HCl 2%. (Table S1). Chitosan in HCl will therefore be systematically used in the rest of this study both for nanoparticle and gold ion dilutions.

Transport Efficiency

As no nanoparticle suspension concentration standard is commercially available, nanoparticle size determinations are classically realized by external calibration with dissolved Au standard solutions. Such calibrations require accurate determination of the transport efficiency. As described by Ranville[21] and co-authors, there are three main calculations of transport efficiency: waste collection, particle size and particle number concentration methods.

The waste method assumes that analyte flow entering the plasma equals the nebulizer uptake flow minus the waste flow which is not the case; a portion of the sample flow is evaporated by the argon gas and the nebulizing chamber concentrates the sample by condensation[22].

The particle size method η_{size} is based on the assumption that nanoparticles remain unchanged between the nebulizer and the plasma entrance whereas solutions are partitioned in the nebulizing chamber. This method is attractive as not requiring suspension concentration measurement but it implies that nanoparticles are totally ionized in the plasma or totally detected whatever their size. This point will be studied in details later.

Finally, particle number concentration transport efficiency (η_{number}), the most widespread method, assumes particle concentration being perfectly known thanks to an independent technique such as SAXS. It is classically calculated as:

$$\eta_{number} = \frac{N_{spk}}{[AuNPS] \times D \times F} \qquad (2)$$

Where N_{spk} is the number of nanoparticle spikes detected with intensity superior to background cutoff (blank mean value + 5σ), [AuNPS] is the nanoparticle number concentration of the suspension deduced from an independent technique e.g. SAXS, D is the analysis duration and F is the nebulizer flow.

The accuracy of SPICPMS depends largely on that of the transport efficiency determination[23]. It is an essential value which is currently rarely evaluated critically. The actual tendency consists in the determination of η_{number} on only one suspension, not certified in particle number concentration and

performed at a single dilution. The uncertainty reported is therefore the repeatability which does not comprehensively evaluate the transport efficiency accuracy.

Table 2. Number transport efficiencies repeability or reproductibility. Nanoparticle concentration for measurement, number of spikes detected, number of different suspension analyzed, total number of measurement, RSD of η_{number} calculated.

Nanoparticles	[AuNPS] p/mL	N_{spk}	Number of suspension analyzed	Total number of Meas^{mt}	RSD (%)
100nm	7646	1700-2100	1	5	4%
60nm	1000-6000	700-1500	3	7	7%
100nm	1500-75000	800-900	6	6	7%
20-100nm	5500	500-800	6	6	20%[a]

We propose to evaluate transport efficiency accuracy in a more complete manner focusing on the influence of size and concentration but restricting our study to gold nanoparticles. This study is based on SAXS determinations. The results are reported in Table 2 and Tables S2-S5. The instrument stability is shown with measurement repeatability evaluated on a 100nm suspension. A RSD value of 4% is obtained. Sampling reproducibility is studied, measuring first 60nm then 100nm suspensions across a range of concentrations. Reproducibility then increases to 7% with no relation between transport efficiency and nanoparticle concentration. This confirms that nanoparticle concentration has no influence on transport in the range studied but shows that the sampling method induces dispersion. . As mentioned above, dilution of nanoparticles suspension is an important issue. In our experience[24], many phenomena can disturb suspension dilution such as nanoparticle destabilization, significant nanoparticle adsorption on vials or pipette tips surfaces or a lack of suspension homogeneity during sampling…. In this work, sampling is realized shortly before analysis by successive weight dilutions (typically 3 or 4) in HCl solution in presence of chitosan to avoid destabilization. Suspensions are shaken for a few minutes before sampling as recommended by the supplier. Sonication, which is most often used, has been discarded here as it can lead to other perturbations like aggregation[24, 25]. The last experiments focus on the influence of nanoparticle size. The use of suspensions of various gold nanoparticle sizes degrade the reproducibility. This is very probably exclusively due to the additional error brought by the concentration determination. It can be deduced from these measures that in this work SPICPMS accuracy can hardly be better than 20% if based on particle number transport efficiency accuracy. It has to be added that this statement doesn't take into account additional errors that can also deteriorate reliability[23].

Calibration

SPICPMS calibration is classically realized with standard solutions but it is also possible to calibrate with nanoparticle suspensions. The method accuracy then depends on those of the suspensions. The variation of signal intensity average versus cubed diameter is shown on Figure 3a and Tables S6. The

figure compares the experimental points in the range of 30 to 150nm with the expected calibration curve calculated from the linear equation bellow:

$$I_{NPS}^{calc} = \frac{M_{SAXS} \times b}{DW \times F \times \eta_{Number}} + a \qquad (3)$$

Where: I_{NPS}^{calc} is the calculated SPICPMS nanoparticle signals average counts, M_{SAXS} is the nanoparticle mass calculated from SAXS diameter measurements, a and b are respectively the standard solution calibration curve intercept and slope, DW is the dwell time and F is the nebulizer flow.

Experimental points, except for the lowest values, appear to be very distant from the expected calibration curve, the experimental variation curve rolling off at high diameters. Deviation from linearity has already been reported[14, 26, 27]. It was suggested that it could be attributed to an incomplete vaporization of nanoparticles in the argon plasma or to detection difficulties[26].

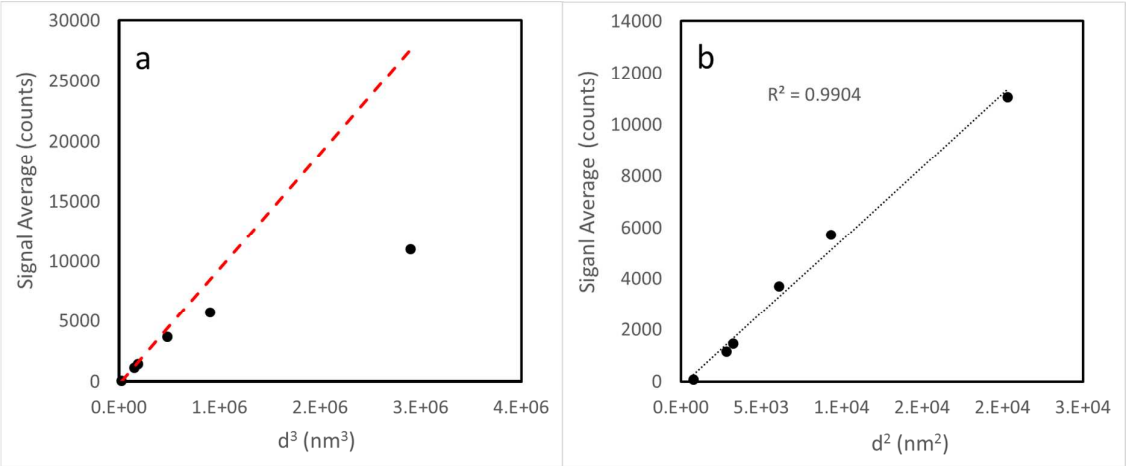

Figure 3. Calibrations curves of gold nanoparticles with diameters of 30, 50, 60, 80, 100 and 150nm versus (a): cubed diameter, dashed line: expected calibration curve calculate from the linear equation 2, (b): square diameter, dotted line: linear regression

Nanoparticle vaporization in the argon plasma can be viewed as a two-stage process: the heat transfer from plasma to particle and the mass transfer from the particle to the plasma[28,29]. In mass transfer limited vaporization, vaporization is controlled by material removal rate from the nanoparticle surface. The particle diameter decreases linearly with time, independently from the particle radius. In heat transfer limited vaporization, the vaporization is limited by the energy flux towards the particle surface. The phenomenon then scales with particle radius squared. In the measurements reported here, nanoparticles signals counts versus diameter squared is linear in the range of 30-150nm apparently fitting with a mass transfer limited vaporization process. (Figure 3b). It can theorized from this result that only an outer shell of the gold core is evaporated, ionized and thus analyzed or that just of an external portion of the ionic cloud is measured by the detector. It has to be pointed out that this

result is coherent with a recent study demonstrating that SPICPMS is sensitive to nanoparticle shape[30].

To better understand these results, the calibration is reproduced at lower RF generator power. In cold plasma conditions, sensitivity is reduced and plasma parameters are modified. At 1000W, the calibration curve versus cubed diameter is surprisingly linear in the range 50-150nm, the 30nm nanoparticles being undetected in these operating conditions. (Figure S1).

To state between plasma issues and incomplete detection, the calibration is reproduced in hot plasma conditions but moving the torch sideways to preserve plasma conditions while diminishing signal amplitude. (Figure S2). Here also, the smallest nanoparticles are again not detected because of the poorer ionic cloud sampling caused by the improper torch alignment with the sampling cone. The calibration curve is linear for low intensity signals (50-100nm) before rolling-off. These results are in agreement with MR Winchester and co-authors who showed that the reduction of sensitivity extended the linear dynamic size range of SPICPMS up to of 200nm-diameter nanoparticles[14].

From these experiments it is then possible to ruleout incomplete vaporization hypothesis. Linearity deviation is thus related to detection issues.

Detection

Secondary electron multiplier detectors have two working modes: counter and analog. Detectors deactivate the counter mode if the number of impacting ions exceed a defined limit. This tripping is performed before a defined delay. If both conditions are met, the detection is operated in the analog mode. If the time limit is exceeded, the detection is realized in the counter mode.

Whatever model of quadrupole ICPMS, detection disorders have already been observed and questioned by several authors. Some stated that in a Gaussian pulse, the signal could rapidly exceed the dynamic range of the detector[26]. The counter / analog tripping has also been accountable for the lack a linearity. The remedy then consisted in diminishing the instrument sensitivity to remain in counting mode[14]. Other authors pointed out that the detector dead time could induce significant errors[31, 32]. To our knowledge, none of these articles proposed a solution to improve the detection of single nanoparticle quadrupole ICPMS without sacrificing sensitivity.

The counter analog tripping timeout is a parameter that can be changed. When analyzing dissolved compounds, signals are roughly constant overtime. The counting threshold timeout is then set to very short delays to protect the detector from deterioration. Detections parameters are typically set to 20µs for the timeout and 25cp for the counting threshold. The counter / analog tripping point reaches then 1 250 000 counts per second. Conversely for single particle detection, the timeout is extended to long delays to avoid untimely tripping of the analog mode, analog mode being less sensitive than counting. In these slow gating conditions, the timeout is typically set to 1000µs and the threshold to 1250cp to not to modify the tripping point value

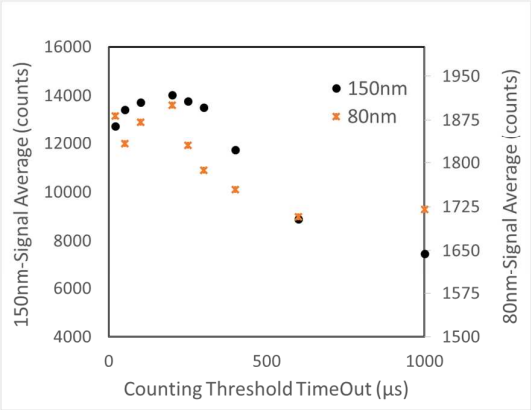

Figure 4. Influence of Counting Threshold Timeout on 150nm and 80nm signal average at constant counter analog tripping point

Figure 4 shows the variation of 150nm and 80nm-diameter gold nanoparticle mean signals versus counter threshold timeout between 20 and 1000µs at constant tripping point. The delay shows an influence on both size of nanoparticles studied. The optimum timeout for both sizes appears to be around 200µs. If the timeout is too short, the detector gates to analog from very small quantities of ions. If it turns out that the total quantity of ions is low, the signal is detected in the analog mode with a lower accuracy or even not detected. On the contrary, if the timeout is too long, the detector keeps to counter mode and a significant part of the signal can be lost. The optimum timeout coincides with the typical rising width of single nanoparticle ion profiles[32]. The detector should therefore gate to analog before the ionic cloud which results from nanoparticle vaporization propagates towards the sampling cone and reaches its maximum amplitude.

If the signal intensity is stable as for dissolved compounds analysis, the relevant parameter is the tripping point value. If the signal is inferior to this value, the detection is realized in counting mode. On the contrary, the analog mode is selected. For transient signal, the tripping point value is not anymore a relevant parameter. The number of counter/analog tripping events has been calculated for each point of Figure 4. (Table S7). For 150nm-nanoparticles, the number of tripping event doesn't exceed 70% of total number of spike detected even if the average signal reaches 2 million of counts per second, a value far above the tripping point value. The number of tripping events has also been calculated at the optimum timeout for the entire set of nanoparticle studied. (Table S8). The results show that counter /tripping can occur largely before the tripping point value. As an example, 80nm-nanoparticle mean signal intensity is about 300 000 counts per second while 56% of the spike events are detected in the analog mode.

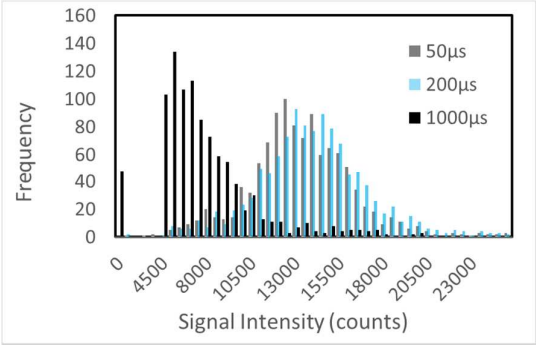

Figure 5. Influence of detection parameters on SPICPMS 150nm-signal distribution

Detection tripping parameters show not only an influence on signal mean value but also on signal distribution diagrams as shown on Figure 5. The figure shows for the slow gating conditions an unsymmetrical long tailing signal distribution which is a distribution shape that is often reported for large nanoparticles[14, 33, 34]. Tuning detection diminishing gating delay improves the distribution. It appears as symmetrical except for a tiny shoulder before the peak. (Figure S3). This shoulder is attributed to missed counter / analog tripping events that could not have been totally eliminated by the detection tuning.

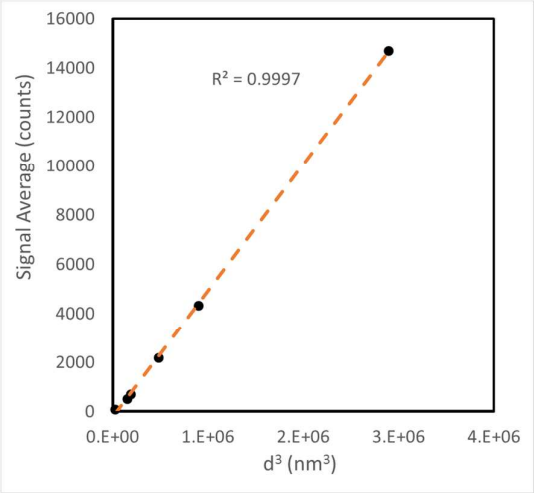

Figure 6. Calibrations curves of gold nanoparticles with diameters of 30, 50, 60, 80, 100 and 150nm versus cubed diameter, dashed line: expected calibration curve calculated from the linear equation 3

To confirm the contribution of the detector timeout tuning, the SPICPMS calibration is renewed in hot plasma in the range 30-150nm. The Figure 6 compares the experimental points in the range of 30 to 150nm with the expected calibration curve calculated from the linear equation 3. (Table S9). With these operating conditions, the variation of nanoparticle signal average with cubed diameter is linear

and data are fully coherent with the theoretical calibration curve. It can added that it seems from these results that dead time correction is unnecessary with our instrument in the signal range studied.

Size Transport Efficiency

If the calibration is linear, it is relevant to calculate transport efficiency basing on signal intensities instead of particle numbers. As shown above, number transport efficiency accuracy can be quite low. η_{number} relies not only on particle number concentration which is not certified but also on the cut-off value distinguishing signal from baseline. This value is chosen by the operator generally as the blank mean intensity + n X σ, with generally $3 \leq X \leq 5$[15, 35]. On the contrary η_{size} avoids two major difficulties, the nanoparticle concentration determination and the accurate dilution process as it is only based nanoparticle signal intensity.

The particle size transport efficiency η_{size} can be defined as the ratio of the nanoparticle mass to the calculated mass obtained from the calibration curve. Theoretically equaling $\eta_{number,}$ it can be calculated by the following Equation 4:

$$\eta_{size} = \frac{M_{SAXS}}{\frac{I_{NPS}^{exp}-a}{b} \times DW \times F} \qquad (4)$$

Where I_{NPS}^{exp} is the experimental SPICPMS nanoparticle signal mean distribution.

Table 3 lists both ηnumber and ηsize values. ηsize average value is fully coherent with ηnumber and its accuracy is improved. In conclusion, particle size transport efficiency ηsize is, according to this study, more relevant than particle number concentration ηnumber even if there seems to be a general acceptance for the latter.

Table 3. Transport efficiencies.

Nanoparticles	η_{number}	η_{size}
30 nm	4.1%	6.0%
50 nm	4.4%	7.2%
60 nm	6.1%	6.6%
80 nm	6.7%	5.4%
100 nm	5.1%	5.1%
150 nm	7.6%	4.8%
Average ± σ	5.7 ± 1.4	5.8 ± 0.9

Size distribution determination

The last part of this work consists in applying the results to the determination of commercial suspensions bought from various suppliers. The first suspension is chosen because of its large size

that is 135nm as announced by the supplier. The second one is a suspension of smaller nanoparticles 40nm to demonstrate the validity of method for various sizes. The third suspension is a monodisperse size suspension of 50nm gold nanoparticles. This sample is chosen to compare the width of diameter distribution by SAXS and SPICPMS.

All suspensions are analyzed by SAXS and fitted by a Gaussian distribution. Mean diameters and standard deviations of the population Gaussian distribution are listed in Table 4. The monodispersity of the samples in diameter is good especially for the 50nm sample as expected, but the measured average sizes are significantly smaller than advertised by sellers.

Table 4. Mean diameters and σ of sample Gaussian distribution by SPICMS and SAXS

	Samples		
	135nm	50nm	40nm
d_{SAXS} (nm)	118.3	48.4	38.2
σ_{SAXS} (nm)	6.6	1.7	4.8
$d_{SPICPMS}$ (nm)	117.9	45.5	37.9
$\sigma_{SPICPMS}$ (nm)	11	5	20
$\Delta\left(\frac{d_{SPICPMS}-d_{SAXS}}{d_{SAXS}}\right)$	-0 3%	-6%	-0.6%

The SPICPMS experiment includes the analysis of three nanoparticles suspensions (60, 100 and 150nm) for η_{size} determination, a standard solution calibration curve, the nebulizer flow and the measurement of the three samples. (Table S10). All signals are fitted by Gaussian distributions, as performed for SAXS. The results are shown in Table 4. SPICPMS Gaussian distribution mean diameters are very consistent with SAXS, except surprisingly for the ultra uniform 50nm sample. The experiment is repeated after one week decreasing the dwell time from 7 ms to 3 ms. Under these operating conditions, the sample concentration is divided by a factor of 2 and the analysis duration is increased from 1200s to 2400s to keep the number of detected nanoparticle unchanged. The Gaussian distribution average diameter remain constant at 45.7 nm with a σ of 5.

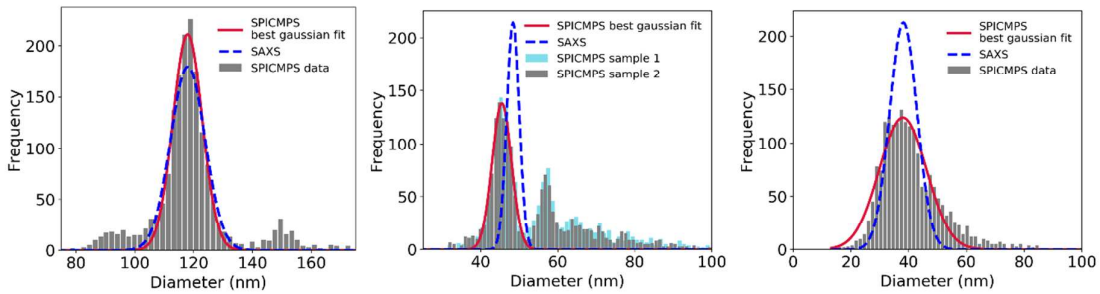

Figure7. SAXS and SPICPMS size distribution histograms and Gaussian fittings for 135nm, 50nm and 40nm-samples from left to right

Figure 7 compares SPICPMS size distribution with both SAXS and SPICPMs fittings. The 135nm and 50nm samples show several well-defined peaks. On the 135nm diagram, a first peak appears slightly before 100nm. This has probably no physical reality. It may be due to a detection artefact not fully eliminated by the detection tuning as explained before. The third peak at about 150nm corresponds to the detection of two nanoparticles. The reason for that can be the presence of two nanoparticles at the same time in the plasma or the analysis of two primary nanoparticles aggregates or the assembling of two nanoparticles trapped in the same chitosan polymeric strand. The experiment performed at smaller dwell time and lower concentration showed no modification of the diameter distribution. This indicates that the peak is not due to a simultaneous presence of nanoparticles in the plasma.

The ultra uniform 50nm-sample shows even more clearly the presence of at least 2 peaks. The second peak at 57nm that is $45.5 \times 2^{(1/3)}$ can be attributed to the analysis of two nanoparticles. Larger assemblies can also be identified at 66, 72 and 78 nm corresponding to 3, 4 and 5 nanoparticles. Aggregation can also be evaluated by SAXS. SAXS diagrams do not show aggregation conversely to SPICPMS. It is therefore probable that these peaks witness the presence of more than one nanoparticle in a chitosan filament.

This phenomena also occurs very probably in the 40nm-sample. In this case, it is more difficult to detect as the nanoparticles are less monodisperse in diameter size. It is nevertheless possible to see a shoulder corresponding to 2 nanoparticles at 48nm.

All diameter distributions are fitted with a Gaussian models. This model is preferred to log-normal for data fitting for two reasons. Gold nanoparticles are classically synthesized by regrowth. There is therefore no physical reason for a nanoparticle distribution tailing to the large size side as it is often applied for distributions of nanoparticles obtained by grinding. The tailing of SPICPMS distribution, such as for the 40nm-sample is very probably mainly due to the convolution of various diameter distributions of one or more nanoparticles.

Fitting SPICPMS signals with Gaussian distributions to establish standard deviations shows measurement spreads to be significantly larger for SPICPMS than for SAXS. This phenomenon has already been observed when comparing SPICPMS with other techniques[36]. It is difficult yet to ascribe the origin of this systematic effect but to the multiplicity of nanoparticle trajectories[37] and spatially varying temperatures conditions in the plasma which are all parameters that may degrade the accuracy.

Acknowledgements:

Maïté Paternostre is acknowledged for the access to the mini electron microscopy platform “TEM-team” (CEA/iBiTec-S). The authors also thank the DIM Analytics of the Region Ile de France and the Plateau de Saclay RTRA program for the IcapQ funding.

Perspectives

A path forward to the resolution of SPICPMs metrology issues is proposed with this comprehensive study. The investigation of the effects reported here should lead to means of SPICPMS accuracy improvements. Considering instrumentation, the stabilization of gold nanoparticle suspension in HCl with chitosan down to very low concentrations shows that ICPMS acquisition speed is not in itself a key issue. The simultaneous signal acquisition over the entire mass range such as performed with ICPTOF[38] is in our opinion of much higher importance. Sensitivity improvement is another essential issue. Sensitivity should be increased to analyze nanoparticles of small size (<15nm) but also nanoparticles composed of light elements such as silicon or aluminum, elements that are largely used in nanostructured materials. Considering methodology, sampling appears as an important feature. It is unfortunately hardly ever studied even if directly impacting accuracy. This study is restricted to gold nanoparticles but it makes significant advances in transport efficiency determination. The next step is logically the extension to other materials than gold. It will necessitate similar full suspension characterization by an independent technique such as reported here with SAXS. It especially implies the availability of large range of sizes of monodisperse nanoparticle suspensions which is very difficult to find commercially except for gold, silver or silica. The synthesis of tailored nanoparticles for analytical purposes is therefore another future challenge. The use of such nanoparticle sets will allow to comprehensively study transport efficiency, addressing in particular the question of a possible influence of nanoparticle elemental composition. The tuning of detector as proposed here can be considered as a contribution. Detection is still an issue that has to be improved to establish SPICPMS as a sufficiently accurate technique to complement SAXS or microscopy. Its main asset is the possible simultaneous elemental measurement over the mass range, SPICMS should therefore in the future be the technique of choice for core shell or multi-elemental nanoparticles, provided once again that the entire nanoparticle is analyzed whatever its size.

Whatever these difficulties, SPICPMS, whether as performed here or in combination with a microdrop generator[40] must be developed because it could offer a unique counting response for many industrial nanomaterial fabrication issues as well as environmental or medical concerns.

References

1. Gaillard, C.; Mech, A.; Rauscher, H. *The Nanodefine Methods Manual, NanoDefine Technical Report D7.6,*; Nanodefine Consortium, Wageningen, 2015.

2. Rasmussen, K.; Rauscher, H.; Mech, A.; Sintes, J. R.; Gilliland, D.; Gonzalez, M.; Kearns, P.; Moss, K.; Visser, M.; Groenewold, M.; Bleeker, E. A. J., Physico-chemical properties of manufactured nanomaterials - Characterisation and relevant methods. An outlook based on the OECD Testing Programme. *Regulatory Toxicology and Pharmacology* **2018,** *92*, 8-28.

3. Guiot, C.; Spalla, O., Stabilization of TiO2 Nanoparticles in Complex Medium through a pH Adjustment Protocol. *Environmental Science & Technology* **2013,** *47* (2), 1057-1064.

4. Zemb, T.; Tache, O.; Ne, F.; Spalla, O., Improving sensitivity of a small angle x-ray scattering camera with pinhole collimation using separated optical elements. *Review of Scientific Instruments* **2003,** *74* (4), 2456-2462.

5. Meli, F.; Klein, T.; Buhr, E.; Frase, C. G.; Gleber, G.; Krumrey, M.; Duta, A.; Duta, S.; Korpelainen, V.; Bellotti, R.; Picotto, G. B.; Boyd, R. D.; Cuenat, A., Traceable size determination of nanoparticles, a comparison among European metrology institutes. *Measurement Science and Technology* **2012,** *23* (12).

6. Bourgeault, A.; Cousin, C.; Geertsen, V.; Cassier-Chauvat, C.; Chauvat, F.; Durupthy, O.; Chaneac, C.; Spalla, O., The Challenge of Studying TiO2 Nanoparticle Bioaccumulation at Environmental Concentrations: Crucial Use of a Stable Isotope Tracer. *Environmental Science & Technology* **2015,** *49* (4), 2451-2459.

7. Degueldre, C.; Favarger, P. Y., Colloid analysis by single particle inductively coupled plasma-mass spectroscopy: a feasibility study. *Colloids and Surfaces a-Physicochemical and Engineering Aspects* **2003,** *217* (1-3), 137-142.

8. Laborda, F.; Bolea, E.; Cepria, G.; Gomez, M. T.; Jimenez, M. S.; Perez-Arantegui, J.; Castillo, J. R., Detection, characterization and quantification of inorganic engineered nanomaterials: A review of techniques and methodological approaches for the analysis of complex samples. *Analytica Chimica Acta* **2016,** *904*, 10-32.

9. Montano, M. D.; Olesik, J. W.; Barber, A. G.; Challis, K.; Ranville, J. F., Single Particle ICP-MS: Advances toward routine analysis of nanomaterials. *Analytical and Bioanalytical Chemistry* **2016,** *408* (19), 5053-5074.

10. Bustos, A. R. M.; Petersen, E. J.; Possolo, A.; Winchester, M. R., Post hoc Interlaboratory Comparison of Single Particle ICP-MS Size Measurements of NIST Gold Nanoparticle Reference Materials. *Analytical Chemistry* **2015,** *87* (17), 8809-8817.

11. PySAXS Software. https://pypi.python.org/pypi/pySAXS.

12. Bressler, I.; Pauw, B. R.; Thunemann, A. F., McSAS: software for the retrieval of model parameter distributions from scattering patterns. *Journal of Applied Crystallography* **2015,** *48*, 962-969.

13. Kalomista, I.; Keri, A.; Galbacs, G., Optimization of plasma sampling depth and aerosol gas flow rates, for single particle inductively coupled plasma mass spectrometry analysis. *Talanta* **2017,** *172*, 147-154.

14. Liu, J. Y.; Murphy, K. E.; MacCuspie, R. I.; Winchester, M. R., Capabilities of Single Particle Inductively Coupled Plasma Mass Spectrometry for the Size Measurement of Nanoparticles: A Case Study on Gold Nanoparticles. *Analytical Chemistry* **2014,** *86* (7), 3405-3414.

15. Peters, R.; Herrera-Rivera, Z.; Undas, A.; van der Lee, M.; Marvin, H.; Bouwmeester, H.; Weigel, S., Single particle ICP-MS combined with a data evaluation tool as a routine technique for the analysis of nanoparticles in complex matrices. *Journal of Analytical Atomic Spectrometry* **2015,** *30* (6), 1274-1285.

16. ISO 17867:2015, P. s. a. S.-a. X.-r. s., s. d.

17. Pauw, B. R.; Kaestner, C.; Thuenemann, A. F., Nanoparticle size distribution quantification: results of a small-angle X-ray scattering inter-laboratory comparison. *Journal of Applied Crystallography* **2017,** *50*, 1280-1288.

18. Tache, O.; Rouziere, S.; Joly, P.; Amara, M.; Fleury, B.; Thill, A.; Launois, P.; Spalla, O.; Abecassis, B., MOMAC: a SAXS/WAXS laboratory instrument dedicated to nanomaterials. *Journal of Applied Crystallography* **2016,** *49*, 1624-1631.

19. Szymanska, E.; Winnicka, K., Stability of Chitosan-A Challenge for Pharmaceutical and Biomedical Applications. *Marine Drugs* **2015,** *13* (4), 1819-1846.

20. Romanazzi, G.; Gabler, F. M.; Margosan, D.; Mackey, B. E.; Smilanick, J. L., Effect of Chitosan Dissolved in Different Acids on Its Ability to Control Postharvest Gray Mold of Table Grape. *Phytopathology* **2009,** *99* (9), 1028-1036.

21. Pace, H. E.; Rogers, N. J.; Jarolimek, C.; Coleman, V. A.; Higgins, C. P.; Ranville, J. F., Determining Transport Efficiency for the Purpose of Counting and Sizing Nanoparticles via Single Particle Inductively Coupled Plasma Mass Spectrometry. *Analytical Chemistry* **2011,** *83* (24), 9361-9369.

22. Schaldach, G.; Berger, L.; Razilov, I.; Berndt, H., Characterization of a cyclone spray chamber for ICP spectrometry by computer simulation. *Journal of Analytical Atomic Spectrometry* **2002,** *17* (4), 334-344.

23. Tuoriniemi, J.; Cornelis, G.; Hassellov, M., Improving the accuracy of single particle ICPMS for measurement of size distributions and number concentrations of nanoparticles by determining

analyte partitioning during nebulisation. *Journal of Analytical Atomic Spectrometry* **2014,** *29* (4), 743-752.

24. Geertsen, V.; Tabarant, M.; Spalla, O., Behavior and Determination of Titanium Dioxide Nanoparticles in Nitric Acid and River Water by ICP Spectrometry *Analytical Chemistry* **2014**.

25. Taurozzi, J. S.; Hackley, V. A.; Wiesner, M. R., Ultrasonic dispersion of nanoparticles for environmental, health and safety assessment - issues and recommendations. *Nanotoxicology* **2011,** *5* (4), 711-729.

26. Lee, W.-W.; Chan, W.-T., Calibration of single-particle inductively coupled plasma-mass spectrometry (SP-ICP-MS). *Journal of Analytical Atomic Spectrometry* **2015**.

27. Ho, K.-S.; Lui, K.-O.; Lee, K.-H.; Chan, W.-T., Considerations of particle vaporization and analyte diffusion in single-particle inductively coupled plasma-mass spectrometry. *Spectrochimica Acta Part B-Atomic Spectroscopy* **2013,** *89*, 30-39.

28. Lee, K. H. Simulation of single particle inductively coupled plasma mass spectrometry. University of Hong Knog, Hong Kong, 2013.

29. Horner, J. A.; Chan, G. C. Y.; Lehn, S. A.; Hieftje, G. M., Computerized simulation of solute-particle vaporization in an inductively coupled plasma. *Spectrochimica Acta Part B-Atomic Spectroscopy* **2008,** *63* (2), 217-233.

30. Kalomista, I.; Keri, A.; Ungor, D.; Csapo, E.; Dekany, I.; Prohaska, T.; Galbacs, G., Dimensional characterization of gold nanorods by combining millisecond and microsecond temporal resolution single particle ICP-MS measurements. *Journal of Analytical Atomic Spectrometry* **2017,** *32* (12), 2455-2462.

31. Strenge, I.; Engelhard, C., Capabilities of fast data acquisition with microsecond time resolution in inductively coupled plasma mass spectrometry and identification of signal artifacts from millisecond dwell times during detection of single gold nanoparticles. *Journal of Analytical Atomic Spectrometry* **2016,** *31* (1), 135-144.

32. Shaw, P.; Donard, A., Nano -particle analysis using dwell times between 10 tis and 70 Its with an upper counting Limit of greater than 3 x 107 cps and a gold nanoparticle detection limit of less than 10 nm diameter. *Journal of Analytical Atomic Spectrometry* **2016,** *31* (6), 1234-1242.

33. Laborda, F.; Jimenez-Lamana, J.; Bolea, E.; Castillo, J. R., Selective identification, characterization and determination of dissolved silver(I) and silver nanoparticles based on single particle detection by inductively coupled plasma mass spectrometry. *Journal of Analytical Atomic Spectrometry* **2011,** *26* (7), 1362-1371.

34. Wang, H.; Chen, B.; He, M.; Hu, B., A Facile Droplet-Chip-Time-Resolved Inductively Coupled Plasma Mass Spectrometry Online System for Determination of Zinc in Single Cell. *Analytical Chemistry* **2017,** *89* (9), 4931-4938.

35. Bolea-Fernandez, E.; Leite, D.; Rua-Ibarz, A.; Balcaen, L.; Aramendia, M.; Resano, M.; Vanhaecke, F., Characterization of SiO2 nanoparticles by single particle-inductively coupled plasma-tandem mass spectrometry (SP-ICP-MS/MS). *Journal of Analytical Atomic Spectrometry* **2017,** *32* (11), 2140-2152.

36. Laborda, F.; Jimenez-Lamana, J.; Bolea, E.; Castillo, J. R., Critical considerations for the determination of nanoparticle number concentrations, size and number size distributions by single particle ICP-MS. *Journal of Analytical Atomic Spectrometry* **2013,** *28* (8), 1220-1232.

37. Bogaerts, A.; Aghaei, M., Inductively coupled plasma-mass spectrometry: insights through computer modeling. *Journal of Analytical Atomic Spectrometry* **2017,** *32* (2), 233-261.

38. Borovinskaya, O.; Hattendorf, B.; Tanner, M.; Gschwind, S.; Guenther, D., A prototype of a new inductively coupled plasma time-of-flight mass spectrometer providing temporally resolved, multi-element detection of short signals generated by single particles and droplets. *Journal of Analytical Atomic Spectrometry* **2013,** *28* (2), 226-233.

39. Ho, K. S.; Lee, W. W.; Chan, W. T., Effects of ionization potential of an element and boiling point of the corresponding oxide on the sensitivity of ICP-MS. *Journal of Analytical Atomic Spectrometry* **2015,** *30* (10), 2066-2073.

40. Borovinskaya, O.; Gschwind, S.; Hattendorf, B.; Tanner, M.; Guenther, D., Simultaneous Mass Quantification of Nanoparticles of Different Composition in a Mixture by Microdroplet Generator-ICPTOFMS. *Analytical Chemistry* **2014,** *86* (16), 8142-8148.